Ambiente & Água - An Interdisciplinary Journal of Applied Science
ISSN 1980-993X – doi:10.4136/1980-993X
www.ambi-agua.net
E-mail: ambi.agua@gmail.com

Efficient removal of aqueous chromium using hydrothermally activated perlite

ARTICLES doi:10.4136/ambi-agua.3103

Received: 10 Aug. 2025; Accepted: 03 Dec. 2025

Berthy Indira Paye-Masco[1]; Beronica Gomez Castañeda[1]; Derly David Ortiz-Romero[1]; Linda Gabriela Quispe-Quispe[1]; Luiz Pereira da Costa[2]; Teresa Cano de Terrones[1]; Lina Graciela Quispe-Quispe[1]*

[1]Departamento Académico de Química. Universidad Nacional de San Agustín de Arequipa, Avenida Independencia, s/n, 04001, Cercado, Arequipa, Peru. E-mail: bpaye@unsa.edu.pe, bgomezcas@unsa.edu.pe, dortizr@unsa.edu.pe, liquispequ@unsa.edu.pe, dcanof@unsa.edu.pe
[2]Centro de Ciências Exatas e Tecnologia. Programa de Pós-Graduação em Química. Departamento de Química. Universidade Federal de Sergipe (UFS), Avenida Governador Marcelo Deda, s/n, CEP:49100-000, São Cristóvão, SE, Brazil. E-mail: lupeco7@hotmail.com
*Corresponding author. E-mail: lquispequi@unsa.edu.pe

Editor-in-Chief: Nelson Wellausen Dias

ABSTRACT

The removal of chromium from wastewater has received considerable attention in recent years due to its harmful environmental effects. This study evaluated the chromium adsorption capacity of activated perlite obtained by a hydrothermal process using 20% NaOH and 30% NaCl. The experiments were performed using a synthetic $Cr(OH)SO_4$ solution containing chromium predominantly as Cr(III), as confirmed by chromium speciation analysis. Adsorption experiments based on a factorial design assessed the effects of initial chromium concentrations (401-1482 mg L^{-1}) and activated perlite dosages (10-30 g L^{-1}). The Langmuir isotherm provided the best fit to the data at 273.15-298 K, yielding a maximum adsorption capacity of 133 mg g^{-1} and a Langmuir constant of 0.09 L mg^{-1}. Kinetic data were consistent with both pseudo-first-order and pseudo-second-order models. Hydrothermal activation increased the cation exchange capacity from 90.57 to 120.52 meq per 100 g. Statistical analysis indicated that chromium removal followed a linear model relative to both initial concentration and adsorbent dosage. These results demonstrate that hydrothermally activated perlite is a promising low-cost and sustainable adsorbent for the removal of Cr(III) from tannery effluents, with potential for large-scale implementation.

Keywords: adsorption isotherm, cation exchange, chromium, factorial design, hydrothermally activated perlite, kinetics.

Remoção eficiente de cromo de soluções aquosas utilizando perlita ativada por tratamento hidrotermal

RESUMO

A remoção de cromo de correntes de águas residuais tem recebido atenção considerável nos últimos anos devido aos seus efeitos ambientais nocivos. Neste estudo, avaliou-se a

capacidade de adsorção de cromo da perlita ativada obtida por um processo hidrotérmico utilizando 20% de NaOH e 30% de NaCl. Os experimentos foram realizados empregando uma solução sintética de $Cr(OH)SO_4$ contendo predominantemente cromo na forma Cr(III), conforme confirmado pela análise de especiação. Ensaios de adsorção baseados em um planejamento fatorial avaliaram os efeitos das concentrações iniciais de cromo (401-1482 mg L^{-1}) e das dosagens de perlita ativada (10-30 g L^{-1}). A isoterma de Langmuir apresentou o melhor ajuste aos dados entre 273,15 e 298 K, resultando em uma capacidade máxima de adsorção de 133 mg g^{-1} e uma constante de Langmuir de 0,09 L mg^{-1}. Os dados cinéticos foram consistentes com os modelos de pseudo-primeira ordem e pseudo-segunda ordem. A ativação hidrotérmica aumentou a capacidade de troca catiônica de 90,57 para 120,52 meq por 100 g. A análise estatística indicou que a remoção de cromo seguiu um modelo linear em relação tanto à concentração inicial quanto à dosagem do adsorvente. Esses resultados demonstram que a perlita ativada hidrotérmicamente é um adsorvente promissor, de baixo custo e sustentável, para a remoção de Cr(III) de efluentes de curtumes, com potencial para implementação em larga escala.

Palavras-chave: cinética, cromo, isoterma de adsorção, planejamento fatorial, perlita ativada hidrotérmicamente, troca catiônica.

1. INTRODUCTION

Chromium is extensively used in various industrial processes, particularly in leather tanning, where hides are treated with chromium salts, vegetable tannins, and formaldehyde (Rai *et al.*, 2025). Among these, the leather tanning industry stands out as a major source of environmental pollution due to the high concentrations of chromium in its effluents (Kerur *et al.*, 2021). The toxicity and mobility of chromium depend largely on its oxidation state. Cr(VI) is highly toxic, carcinogenic and mutagenic, and primarily originates from anthropogenic sources. Because of its severe impact on human health and ecosystems, regulatory agencies have established strict limits for total chromium concentrations in drinking water, typically around 0.05 mg L^{-1} (Vaiopoulou and Gikas, 2020). Several technologies have been developed for chromium removal from industrial effluents, including ion exchange (Leonard *et al.*, 2023), membrane filtration (Njoya *et al.*, 2021), and adsorption (Neolaka *et al.*, 2022). However, these methods often face limitations regarding efficiency, cost, or scalability. Among them, adsorption has emerged as a promising approach, especially when using activated carbon, due to its high surface area and excellent adsorption properties (Teweldebrihan and Dinka, 2025). In addition, other low-cost materials, such as fly ash (Feng *et al.*, 2024), clays (Petrović *et al.*, 2023), modified carbons (Taye *et al.*, 2023; Zahakifar *et al.*, 2024) and zeolites (Álvarez *et al.*, 2021) have been explored.

Zeolites offer notable environmental advantages in removing contaminants from water, soil, and air (Hu *et al.*, 2021; Król and Magdalena, 2020). However, their performance may be hindered by the presence of impurities in natural materials, motivating the search for alternative adsorbents or the development of synthetic zeolites derived from aluminosilicate-rich sources such as expanded perlite (Kasai *et al.*, 2019). Hydrothermal synthesis is a widely used method for activating aluminosilicate materials by treating them with alkaline solutions under controlled conditions (Hou *et al.*, 2023; Painer *et al.*, 2022). The resulting products depend on the raw material's chemical composition and the synthesis parameters such as temperature, pressure, and reaction time (Tang *et al.*, 2022). The availability of silica and alumina is crucial for zeolite formation, making hydrothermal treatment an effective strategy to improve adsorbent performance (Bizualem *et al.*, 2025). Expanded perlite is a naturally occurring volcanic glass composed primarily of amorphous aluminosilicates, with SiO_2 and Al_2O_3 as its

major components (Kotwica *et al.*, 2017). It also contains low levels of impurities and possesses favourable properties such as low density, high porosity, thermal insulation, and chemical resistance (Kasai *et al.*, 2018).

Given the need for cost-effective and efficient adsorbents for chromium removal, this study investigates the adsorption capacity of hydrothermally activated perlite at the laboratory scale. Expanded perlite, widely used in agriculture for its porosity and water retention, was selected as the precursor material. The adsorbent was prepared through hydrothermal activation, a process that involves treating the material under high-temperature and high-pressure aqueous conditions to enhance its structural and surface properties, improving its adsorption efficiency. The modified perlite was then evaluated under batch conditions using a factorial experimental design. A synthetic solution of $Cr(OH)SO_4$ was employed to simulate wastewater from tanning processes.

2. MATERIAL AND METHODS

The experimental methodology involved the characterization of commercial expanded perlite (Knauf brand), followed by its hydrothermal activation and evaluation of its chromium adsorption capacity. $Cr(OH)SO_4$ was provided by Chongqing Minfeng Chemical and used to prepare synthetic chromium solutions.

2.1. Characterization of Expanded Perlite

To characterize the expanded perlite, a morphological analysis was performed using a Scanning Electron Microscope (SEM) (TESCAN VEGA 3, operated at 30 kV). SEM analysis was conducted at the Federal University of Amazonas. Sample preparation involved fixing the calcined powder onto carbon tape mounted on an aluminium stub. Prior to imaging, the sample was sputter-coated with a thin layer of metal using a Bal-Tec SCD 050 Sputter Coater. Additionally, crystallographic characterization was performed using an X-ray diffractometer (Shimadzu XRD-7000). Fourier-transform infrared spectroscopy (FTIR) analysis was conducted at the Faculty of Sciences of the National University of Engineering (UNI) using an IRPrestige-21 SHIMADZU spectrometer equipped with a DLATGS detector and optical components. The spectra were recorded at a resolution of 4 cm^{-1} and were scanned in the range of 650 cm^{-1} to 4000 cm^{-1}. This analysis was used to characterize the types of chemical bonds present in both the expanded and hydrothermally activated perlite samples.

2.2. Activation of expanded perlite

The expanded perlite was first prepared by crushing and classifying the raw mineral, followed by washing to remove impurities and sieving through a 500-mesh screen. The sieved material was then expanded by heating in a rotary kiln and subsequently crushed. The expanded perlite was subjected to hydrothermal treatment using a 30% (w/v) NaCl solution and a 20% (w/v) NaOH solution under constant stirring at 700 rpm and 95°C for 2 hours. The activated perlite was subsequently filtered, thoroughly washed with distilled water, and dried in an oven at 120°C for 12 hours (Tang *et al.*, 2022).

2.3. Determination of Cation Exchange Capacity (CEC)

The cation exchange capacity (CEC) was determined using the method proposed by (McConnell *et al.*, 1974). In this procedure, 2 g of the sample were mixed with 50 mL of 2 N HCl and left to stand for 24 hours. After this period, the mixture was centrifuged at 2000 rpm for 5 minutes. The supernatant was filtered, and the solid residue was washed with 80 mL of saturated NaCl. Subsequently, five drops of phenolphthalein indicator were added and the solution was titrated with 0.1 M NaOH until a persistent pink colour appeared.

The cation exchange capacity was calculated using the following Equation 1:

$$CEC\left(\frac{m_{eq}}{100\ g}\right) = \frac{(mL_m - mL_b)N(100+Pw)}{Pm} \quad (1)$$

Where: mL_m is the volume in mL of NaOH used in the titration, mL_b is the volume in mL of NaOH used in the blank titration, N is the normality of the NaOH, Pw is the moisture content of the sample and Pm is the weight in g of the sample.

2.4. Determination of removal capacity of the activated perlite

Batch adsorption experiments were conducted at room temperature using sterilized 100 mL screw-capped bottles. The synthetic Cr(III)-contaminated solution was prepared in the laboratory by dissolving $Cr(OH)SO_4$, a reagent commonly used in the tannery industry. The synthetic solution was prepared from $Cr(OH)SO_4$, which contains chromium only in the trivalent state. Under the experimental pH conditions (8-8.15) and the measured ORP, the Cr–H_2O speciation diagram indicates that only Cr(III) species are thermodynamically stable. No oxidants capable of generating Cr(VI) were present, and analytical verification confirmed its absence throughout the study. To evaluate the Cr(III) removal from the contaminated solutions, a factorial experimental design was employed with two factors and three central point replications. The first factor was the initial Cr(III) concentration in aqueous solution, with lower and upper limits of 401 and 1482 mg L^{-1}, respectively. The second factor was the dosage of activated perlite, with limits of 10 and 30 g L^{-1}. The mixture of solution and adsorbent was agitated using a SK-O330-PRO variable-speed orbital shaker at 520 rpm and stirred until equilibrium was reached after approximately 8 hours. After the contact time, the treatment mixtures were filtered and analysed. The equilibrium time was determined from kinetic tests in which residual concentration was sampled every 2 h. Kinetic tests indicated stabilization of solution concentration and adsorption capacity at 8 h under the studied conditions. For the adsorption kinetics experiments, the same procedure was followed, but samples were collected every two hours to monitor the variation in Cr(III) concentration over time. The analytical determination of Cr(III) concentration in aqueous solution was carried out by Atomic Absorption Spectroscopy, following EPA Method 218.1 (Revision 3.0, 1986), Chromium by Atomic Absorption, Direct Aspiration.

3. RESULTS AND DISCUSSION

The discussion of this study is structured in two main parts. The first focuses on the morphological and crystallographic characterization of the activated perlite. The second part presents the experimental evaluation of the chromium removal capacity through batch adsorption experiments.

3.1. Characterization of Expanded and Activated Perlite

Figure 1(a) shows the morphology of the expanded perlite before hydrothermal treatment, where the glassy structure exhibits a characteristic honeycomb-like texture (de Oliveira *et al.*, 2019). In contrast, Figure 1(b) displays the morphology of the material after activation, referred to as activated perlite, which presents irregular lamellar grains dispersed with compact surfaces and varying particle sizes, indicating the formation of zeolite-type structures (da Silva Filho *et al.*, 2017).

Figure 2(a) presents the X-ray diffraction (XRD) pattern of expanded perlite, which exhibits a broad diffuse halo centred around $2\theta \approx 22.28°$, without the presence of sharp or intense peaks. This pattern is characteristic of an amorphous structure, indicating that the material lacks long-range crystallographic order. The diffuse hump is typically associated with the presence of disordered silicate networks, common in thermally expanded aluminosilicate materials such as expanded perlite (da Silva Filho *et al.*, 2017; Pioquinto García, 2018). In

contrast, Figure 2(b) shows the diffractogram of activated perlite, where several distinct diffraction peaks are observed at 2θ values of 22.46°, 24.04°, and particularly 27.72°. These features suggest partial crystallization or surface ordering induced by the activation treatment. The peak at 27.72° may correspond to the formation of crystalline phases such as quartz or other silicate structures that are typically formed during chemical or thermal activation processes (Tang *et al.*, 2022). The emergence of these peaks indicates that the activation process has led to structural rearrangements and nucleation of crystalline domains within the initially amorphous matrix. This transformation from an amorphous to a partially crystalline structure may significantly influence the pozzolanic reactivity and ion exchange capacity of the material, potentially enhancing its performance as a supplementary cementitious material or as an alkali-activated precursor.

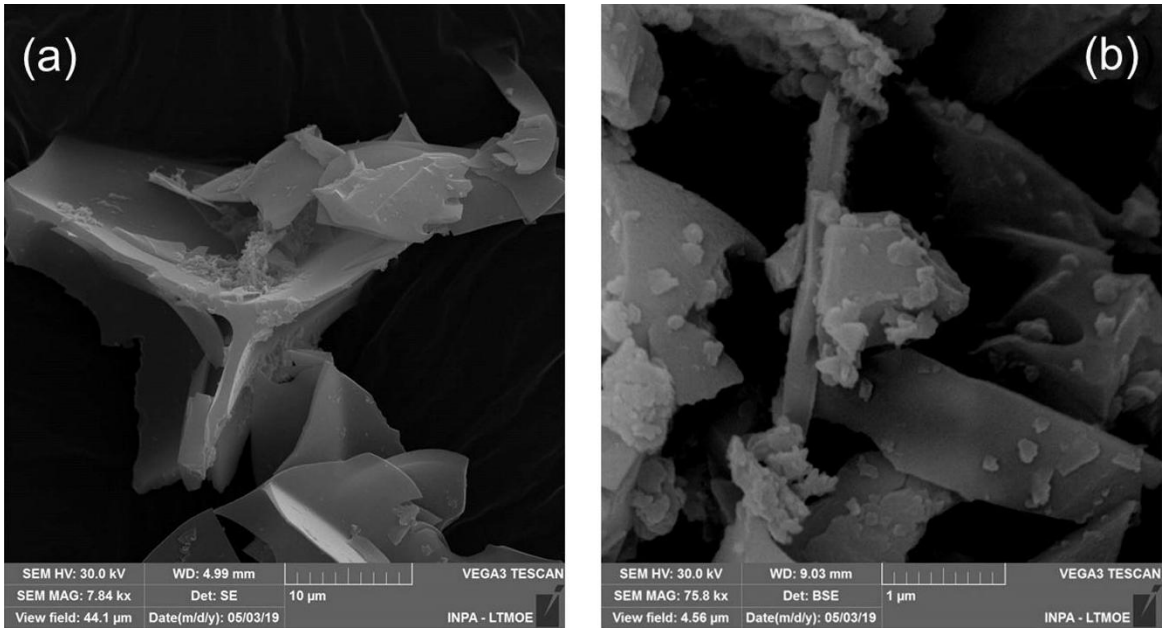

Figure 1. Electron scanning micrographs of (a) expanded perlite and (b) activated perlite (Laboratory of Pre-Packaging and Scientific Metrology - COPREM / INMETRO-Brazil).

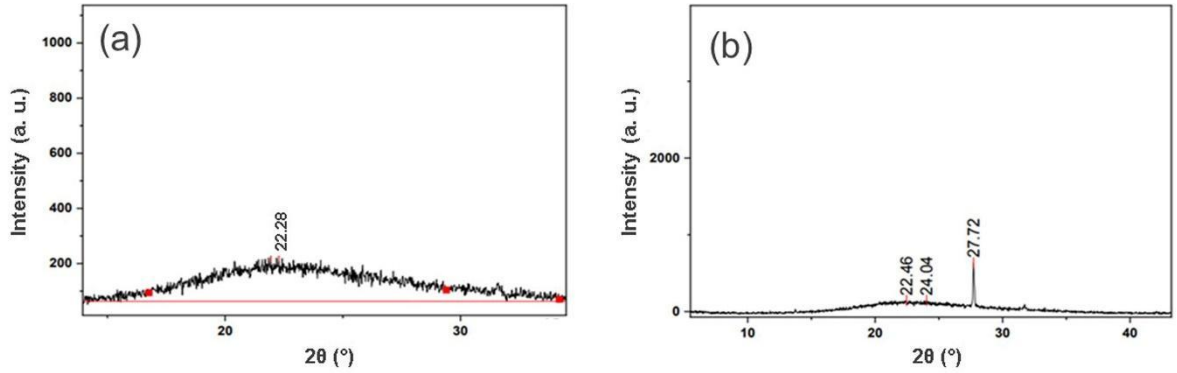

Figure 2. X-ray diffractogram of (a) expanded perlite and (b) activated perlite.

FTIR spectroscopy confirmed the presence of chemical bonds in the expanded perlite and activated perlite structure. The FTIR spectrum of the expanded perlite sample showed absorption bands at 780, 1000 and 1639 cm^{-1} (Figure 3). The peaks observed in the range of 773 to 788 cm^{-1} were the result of stretching vibrations of the Si-O groups (Parra-Huertas *et al.*, 2023). The bands between 962 and 1010 cm^{-1} were due to stretching vibrations in the Si-O-M groups (M: Al or Si). The symmetric and asymmetric Si-O stretching bands were observed to have similar values and appearance than those in previous studies (Moradi *et al.*, 2022).

The transmittance values of expanded perlite and activated perlite at 780 and 1000 cm^{-1} were similar. The peaks around 1639 cm^{-1} (between 1600-1650 cm^{-1}) for activated pearlite were attributed to bending vibrations of O-H groups originating from water molecules (Król *et al.*, 2014). A slight band elevation between 3350 and 3500 cm^{-1} is attributed to Si-OH bonds and hydroxyl (-OH) groups (Legorreta-García *et al.*, 2024). The decrease in the full width at half height of the most intense band located at approximately 1054 cm^{-1} indicates an increasing proportion of crystalline phases with increasing synthesis temperature (Srivastava *et al.*, 2013). The results of FTIR analysis were consistent with previous studies (Wanyonyi *et al.*, 2024).

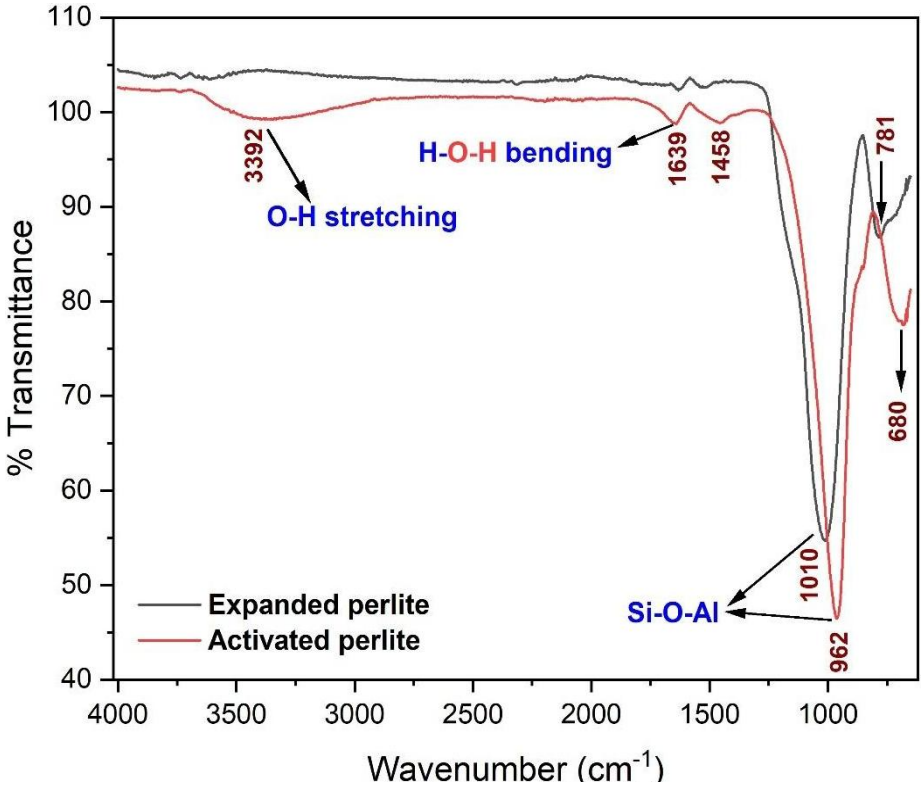

Figure 3. FTIR spectra of expanded perlite and activated perlite samples.

3.2. Cation Exchange Capacity of Expanded and Activated Perlite

The cation exchange capacity (CEC) of the material showed a notable increase following the activation treatment. Specifically, the CEC rose from 90.57 meq per 100 g in the untreated expanded perlite to 120.52 meq per 100 g in the activated (synthetic) perlite. This enhancement suggests a significant improvement in the material's ability to exchange cations, which is a key property for applications in environmental remediation, catalysis and ion removal processes. According to Huanca *et al.* (2018), a CEC value exceeding 120.00 meq per 100 g is indicative of effective ion exchange behaviour. CEC is one of the principal parameters used to evaluate the performance and quality of zeolitic and aluminosilicate-based materials. It provides a quantitative measure of the number of exchangeable cations that a material can retain per unit mass. Higher CEC values are often associated with increased surface reactivity and the presence of more structurally ordered or accessible exchange sites. As noted by Zijun *et al.* (2021), variations in CEC are also indicative of differences in the type and degree of crystallinity of the zeolitic phases present in the material. Therefore, the increase in CEC observed after activation may reflect both a modification of the surface chemistry and the formation of more reactive or crystalline structures, in agreement with structural analyses.

The treatment with NaOH/NaCl induces partial disruption of the aluminosilicate framework of perlite, leading to an increased density of surface –OH groups and enhanced

accessible surface area and porosity. Additionally, Na^+ ions exchange with native cations, homogenizing surface charge and expanding the number of available active sites. These modifications elevate the cation exchange capacity (CEC) and strengthen both electrostatic and ion-exchange interactions, resulting in improved adsorption performance (Painer *et al.*, 2022).

3.3. Activated perlite removal capacity

The adsorption study makes possible the determination of the degree of chromium remotion and the sensitivity of the process in relation to the concentration of solute. Further, to determine the adsorption rate or the time required to reach a certain separation, it is necessary to determine the adsorption kinetic model. Therefore, to determine the chromium removal capacity of the activated perlite, the following models were tested: the adsorption isotherm of activated perlite, kinetics of chromium removal by activated perlite, correlation model of the effects of chromium concentration and activated perlite dose on the removal of chromium from the effluent.

3.4. Adsorption isotherm of activated perlite

From the experimental chromium adsorption tests onto activated perlite, the equilibrium chromium concentration (c_e) and the chromium mass adsorbed per gram (mg g^{-1}) of adsorbent at equilibrium (q_e) values were calculated using the Equation 2:

$$q_e = \frac{(C_0 - C_e)V}{m} \quad (2)$$

Where C_0 is the initial concentration of chromium in the solution (mg L^{-1}), V is the volume of the solution (L) and m is the mass of the adsorbent (g). Two isotherm models, Langmuir and Freundlich, were adjusted to the data for q_e listed in Table 1.

Table 1. Results of batch adsorption experiments using hydrothermally activated perlite. The experimental adsorption capacity (q_e), as well as modelled values from the Langmuir (q_{e_L}) and Freundlich (q_{e_F}) isotherms, were evaluated within a temperature range of 273.15-298 K.

Activated Perlite	**Cr in Solution**		**Cr-Removal**	**Adsorption Capacity**		
Dose	Initial C_0 (mg L^{-1})	Remaining C_e (mg L^{-1})		q_e	q_{e_L}	q_{e_F}
g L^{-1}	mg L^{-1}		%	mg g^{-1}		
10	400.8	1.38	99.66	39.94	14.44	28.64
30	400.8	0.61	99.85	13.34	6.79	22.23
10	500	0.22	99.96	49.98	2.51	16.21
10	550	0.40	99.93	54.96	4.57	19.51
10	600	0.43	99.93	59.96	4.97	19.95
10	650	0.63	99.90	64.94	7.07	22.46
20	1071	6.13	99.43	53.24	46.72	45.47
20	1071	4.05	99.62	53.35	35.03	39.99
20	1071	6.97	99.35	53.20	50.69	47.31
10	1482	199	86.57	128.30	126.10	133.73
30	1482	20.5	98.62	48.72	85.77	66.11

The Langmuir isotherm was adjusted to the data for q_e listed in Table 1 and was defined by the following Equation 3:

$$q_e = \frac{q_{max} K_L C_e}{1 + K_L C_e} \quad (3)$$

Where q_{max} is the maximum adsorption capacity (mg g^{-1}), and K_L is the adsorption coefficient (L mg^{-1}). This model assumes monolayer adsorption onto the surface containing a finite number of identical sorption sites, and according to this model, adsorbed molecules cannot move across the surface or interact with each other (Nasief *et al.*, 2021).

The Freundlich isotherm was adjusted to the data for q_e listed in Table 1 and was defined by the following Equation 4:

$$q_e = K_F (C_e)^{\frac{1}{n}} \quad (4)$$

Where K_F and 1/n indicate the adsorption capacity and the adsorption intensity of the respective system. This model assumes a non-ideal adsorption on heterogeneous surfaces in a multilayer coverage which suggests that stronger binding sites are occupied first, followed by weaker binding sites (Lagos, 2016).

The efficiency of the fitting (r^2) after applying curve fitting technique and the parameters (q_{max}, K, and n) defining both isotherms, Langmuir and Freundlich, are shown in Table 2. By comparison of the r^2 coefficients, it can be concluded that Langmuir is the model that best describes the chromium adsorption capacity of the synthetic perlite, since its coefficient of determination was higher. These values indicate the applicability and viability of synthetic perlite for the removal of total chromium and the description of the absorbent since it forms a monolayer on its surface and interacts with the active sites of the perlite (Asanu *et al.*, 2022).

Table 2. Summary of the Fitting Parameters of the Langmuir (KL) and Freundlich (KF and n) Isotherm Models in the Temperature Range of 273.15-298 K.

Langmuir model			Freundlich model		
q_{max}	K_L	r^2	K_F	n	r^2
(mg g^{-1})	(L mg^{-1})	-	(mg g^{-1}) (mg L^{-1})$^{-1/n}$	-	-
133.3	0.09	0.9773	25.92	3.2	0.7797

Figure 4 shows graphically the efficiency of the fitting curve of the experimental data with the Langmuir model.

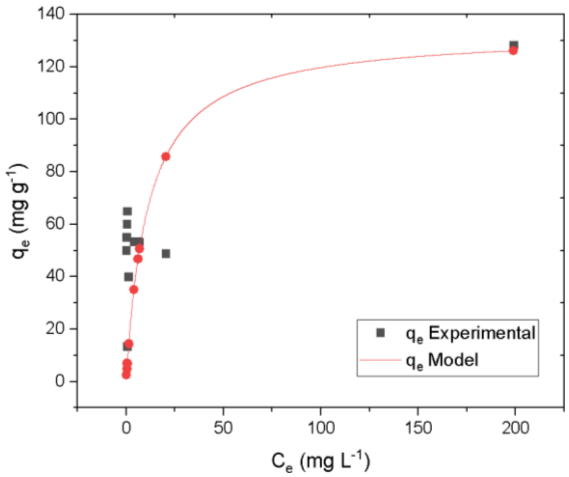

Figure 4. Langmuir model for chromium adsorption using activated perlite.

In accordance to the shape of the isotherm, the equilibrium parameter R_L of the Langmuir model was used to evaluate the adsorption (Islam *et al.*, 2022) and was calculated with the following Equation 5, which uses the initial concentration C_0 of the process:

$$R_L = \frac{1}{1+K_L C_0} \quad (5)$$

Where C_0 is considered as the reference concentration for equilibrium C_e, such that $C_e < C_0$ in the range of C_e concentrations. Furthermore, C_e and C_0 must comply with the Langmuir equation. The interpretation of the equilibrium parameter is given in Table 3:

Table 3. Interpretation of the Langmuir Equilibrium Parameter (R_L) Indicating the Type of Isotherm in the Temperature Range of 273.15-298 K.

	Irreversible	Favourable	Unfavourable
R_L	0	between 0-1	>1

Table 4 shows the results of the R_L calculation for the concentrations evaluated. The R_L values range between 0 and 1, showing to be favourable in the range of concentrations considered, which means that there is a high affinity between adsorbate - adsorbent.

Table 4. R_L values for initial chromium concentrations C_0.

C_0 (mg L^{-1})	400.8	1071	1482
R_L	0.030	0.010	0.007

Additional tests performed with real tannery wastewater confirmed the practical applicability of the process. Despite the presence of organic matter, suspended solids, and competing ions, chromium concentrations of approximately 2500 mg L^{-1} were reduced by more than 90% after 8 h of contact. These results demonstrate that the adsorption system remains effective under complex real-effluent conditions and support the feasibility of scaling the process for industrial applications.

As summarized in Table 5, the maximum adsorption capacity obtained in this study (133 mg g^{-1}) is comparable to or higher than values reported for other low-cost adsorbents commonly evaluated for chromium removal. For Cr(III), hydrothermally activated perlite shows a markedly superior performance compared to materials such as biochars from palm residues and activated chitosan, which exhibit significantly lower adsorption capacities. A broader comparison including Cr(VI) adsorbents is also provided to contextualize the position of activated perlite among low-cost materials; however, Cr(III) and Cr(VI) are reported together with clear indication of their contaminant type, since their adsorption mechanisms differ fundamentally due to their cationic and anionic speciation. Even when contrasted with high-performing Cr(VI) sorbents, activated perlite remains competitive while offering simpler preparation, lower cost, and greater scalability. These attributes support its suitability as an efficient, accessible, and sustainable adsorbent for Cr(III) removal from tannery wastewater.

Table 5. Comparison of adsorption capacities of low-cost adsorbents for chromium removal.

Adsorbent	Chromium species	q_{max} (mg g^{-1})	References
Activated perlite (this study)	Cr(III)	133	This work
Biochar from palm residues	Cr(III)	51.72	Hashem *et al.* (2024)
Activated chitosan	Cr(III)	41.5	Zuo and Balasubramanian (2013)
Biochar from *Peganum harmala* seeds	Cr(VI)	53.48	Khosravi *et al.* (2018)
Coffee-ground biochar	Cr(VI)	30.66	Tian *et al.* (2024)
Cationic modified rice husk	Cr(VI)	42.37	Lala *et al.* (2023)
Activated carbon (Rumex abyssinicus)	Cr(VI)	19.35	Abewaa *et al.* (2024)
Modified clay	Cr(VI)	2.73	Corne *et al.* (2019)
Activated carbon (chia stems)	Cr(VI)	2.08	Bayisa *et al.* (2021)

3.5. Adsorption Kinetic Studies

Kinetic models have been proposed to determine the mechanism of the adsorption process which provided useful data to improve the efficiency of the adsorption and feasibility of process scale-up (Avola *et al.*, 2023). To evaluate the kinetic parameters, pseudo-first order and pseudo-second order models were fitted to analyse the experimental kinetic data shown in Table 4. The pseudo-first-order Equation 6 is expressed as:

$$\left(\frac{q_e - q}{q_e}\right) = exp(-k_1\, t) \tag{6}$$

Where q represents the amount of adsorbed chromium per mass of activated perlite (mg g^{-1}) at equilibrium at a certain time t and k_1 is the first-order rate constant (min^{-1}). On the other hand, the pseudo-second-order Equation 7 is expressed by:

$$\frac{t}{q} = \frac{1}{k_2 q_e^2} + \frac{1}{q_e}\, t \tag{7}$$

Where k_2 is the second-order rate constant (g mg^{-1} min^{-1}).

Using the Equation 3 and the equilibrium concentration C_e for this batch kinetic test of 7.36 mg L^{-1} reached after 8 hours (see Table 6), the equilibrium adsorption capacity, q_e, was 49.15 mg g^{-1}.

Table 6. Experimental kinetic data from a batch experiment, (C_0 = 1482 mg L^{-1}; mass of activated perlite added m = 3 g in a volume of solution of V = 100 mL).

Time (t)	Concentration (c)	Adsorption capacity (q)
(h)	(mg L^{-1})	(mg g^{-1})
0	1482	0.00
2	600	29.40
4	286	39.87
6	7.77	49.14
8	7.36	49.15

As shown in Table 6, the Cr(III) concentration in the aqueous phase decreases rapidly during the first hours and tends to stabilize between 6 and 8 hours, where only a minimal change

in concentration is observed. This stabilization indicates that the adsorption process reached equilibrium at approximately 8 hours. This observation was confirmed by the kinetic profile (see Figure 5), where no significant additional adsorption occurred beyond this period, suggesting that equilibrium conditions were achieved.

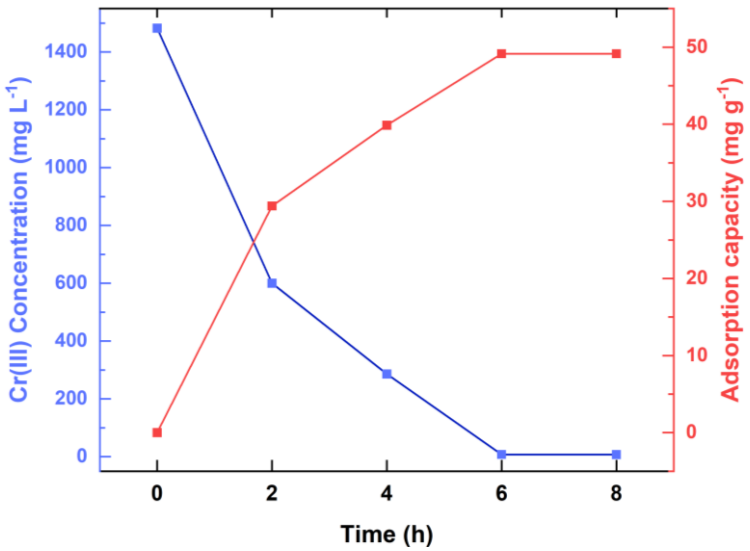

Figure 5. Variation of Cr(III) concentration and adsorption capacity as a function of contact time (adsorbent dosage = 30 g L^{-1}, T = 298 K, pH = 8.15).

The kinetic parameter k of the adsorption process was determined by fitting the models expressed by Equations 6 and 7 to the experimental data. The results of this fitting curve are shown in Figure 6.

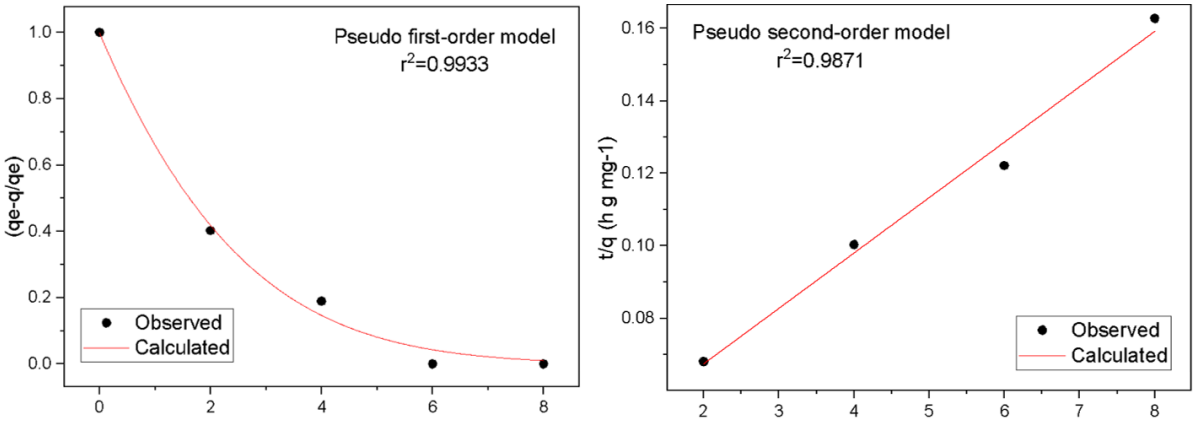

Figure 6. The pseudo-first and pseudo-second order models fitted to the experimental kinetic data shown in Table 7.

And the kinetic parameter k resulting from the fitting is shown in Table 7 for both models.

Table 7. Kinetic parameter for the chromium adsorption by activated perlite.

Model	K	Coefficient r^2
Pseudo first order	0.4655 (h^{-1})	0.9933
Pseudo second order	0.0375 (g mg^{-1} h^{-1})	0.9871

After analysing the determination coefficient r^2 of both models, it was observed that there is not a great difference, as both models predict the adsorption kinetics for chromium onto activated perlite in good agreement with the experimental data (Chanda *et al.*, 2022) (Table 7; see Figure 6).

The adsorption of Cr(III) is strongly pH-dependent: under acidic conditions, the predominance of soluble species such as Cr^{3+} and $CrOH^{2+}$ reduces adsorption due to competition with protons. At neutral to slightly basic pH, surface deprotonation and the formation of chromium hydroxides promote complexation and retention (Huang *et al.*, 2021).

3.6. Correlation of the chromium concentration in aqueous phase with time

In this study, the experimental data presented in Table 6 were adjusted using the chromium concentration in the aqueous phase (c) instead of the adsorption capacity (q), which is the most reported parameter in literature. This choice was made because the residual concentration reflects the solution's purification degree in a direct manner, allowing for a clearer interpretation of the chromium removal by hydrothermally activated perlite's kinetic behavior, especially in the earlier stages of the process.

The adjustment of the data resulted in an excellent correlation, described by an exponential function with a determination coefficient of 0.9927, which confirms that the model adequately describes the observed experimental trend. The function describing the declining concentration with time is expressed as Equation 8:

$$C = a_1 exp(-a_2 t) \tag{8}$$

Where the adjustment parameters are a_1 = 1487.09 and a_2 = 0.4607. Figure 7 shows that the rate of change of the remaining concentration of chromium in the solution gradually decreases in the first hours until it reaches equilibrium (adsorption rate = 0) after 8 hours. After this time, the concentration of chromium in dissolution practically remains constant. At equilibrium, the removal of chromium by adsorption reaches a value of 99%.

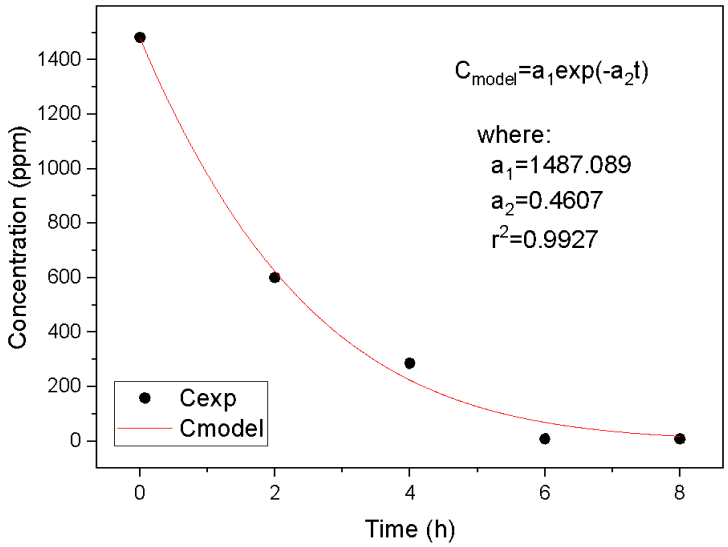

Figure 7. The kinetic adsorption of chromium onto the activated perlite shows an exponential decline of the concentration.

Activated perlite exhibits a moderate regeneration potential; desorption studies have reported that it can be reused for up to 10 cycles before experiencing a significant loss of capacity. This indicates that, although it is economically viable and more sustainable than

single-use adsorbents, maintaining its efficiency over time may require chemical or thermal regeneration strategies (Khoshraftar *et al.*, 2023).

3.7. Correlational model of factors affecting chromium adsorption by activated perlite

The adsorption process is generally affected by factors such as adsorbate concentration, adsorbent dosage, ionic activity of the solution (interference from other ions), temperature, pH, time and type of operation, batch or continuous, among others. For simplicity, in this study, the effect of the initial concentration of the adsorbate (chromium concentration) and the dosage of the adsorbent (activated perlite) on the removal of chromium from the effluent will be evaluated. For this, a laboratory-scale test design (batch) was defined following a factorial design of 2^2 plus 3 replications at the central point, to obtain a mathematical model that can determine the significance of the two factors over the chromium removal by using activated perlite as adsorbent.

The developed model not only allows the evaluation of the influence of the initial chromium concentration and the dose of the activated perlite on the metal removal, but it also enables the optimization of the adsorption process performance. In this manner, the adequate amount of activated perlite to be added can be estimated depending on the chromium concentration present in the effluent, guaranteeing efficient use of the adsorbent and maximum chromium removal.

The data in Table 1 underwent a statistical analysis with the software "Statgraphics Centurion" (as experimental variables: Dose for dose of activated perlite and c_0 for initial concentration of chromium; and as response variable: q_e for the adsorption capacity at equilibrium), which yielded the Pareto diagram (Figure 8) that shows that the dose of activated perlite (B) and the concentration of chromium (A) have a significant effect on the removal percentage with a 95% confidence. However, the interaction (AB) between adsorbent dose and concentration causes the removal percentage to decrease, showing an antagonism between the two variables.

ANOVA results indicate that the factors evaluated significantly influence the adsorption process: both the initial concentration and the adsorbent dose exhibit highly significant effects, with $F = 3460.67$ ($p = 0.0003$) and $F = 51806.49$ ($p < 0.0001$), respectively. Moreover, their interaction is statistically significant ($F = 1231.95$; $p = 0.0008$), confirming that both factors jointly affect the response. Although a significant lack of fit was observed, the minimal pure error (0.0037) supports the reproducibility of the experiment and validates the statistical significance of the model.

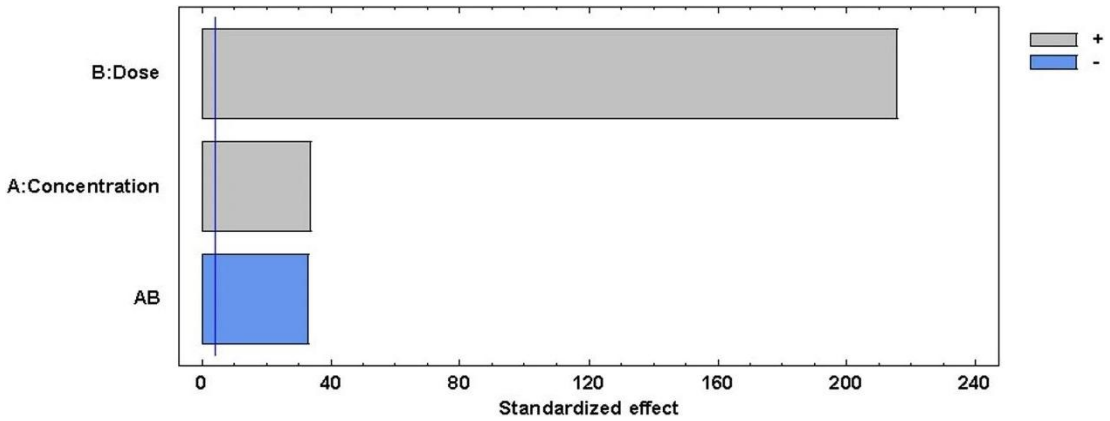

Figure 8. Standardized Pareto chart for removal of chromium in percentage (B: dose of activated perlite and A: initial concentration of chromium in the aqueous phase).

In regards to the statistical model relating the two factors (chromium concentration and activated perlite dosage), the following model was obtained Equation 9:

$$\%\ Removal\ of\ Cr = 74.7596 + 0.0072\ (A) + 8.7807\ (B) + 0.0020\ (A)\ (B) \quad (9)$$

The adjustment of the model yielded a determination coefficient of 0.7309, which means that the results of the chromium removal tests by adsorption on the activated perlite are explained by 73.09% by the chromium concentration and the activated perlite dose. Figure 9 shows the graphic representation of the model expressed by Equation 9, and it can be observed that for an incremental variation in the chromium concentration, a higher dosage of activated perlite is required to obtain maximum effluent removal. Also, it can be deduced from Figure 9 that the maximum chromium removal can be reached for extreme conditions, maximum variation in concentration (1480 mg L^{-1}) and maximum activated perlite dosage (30 g L^{-1} of activated perlite in water).

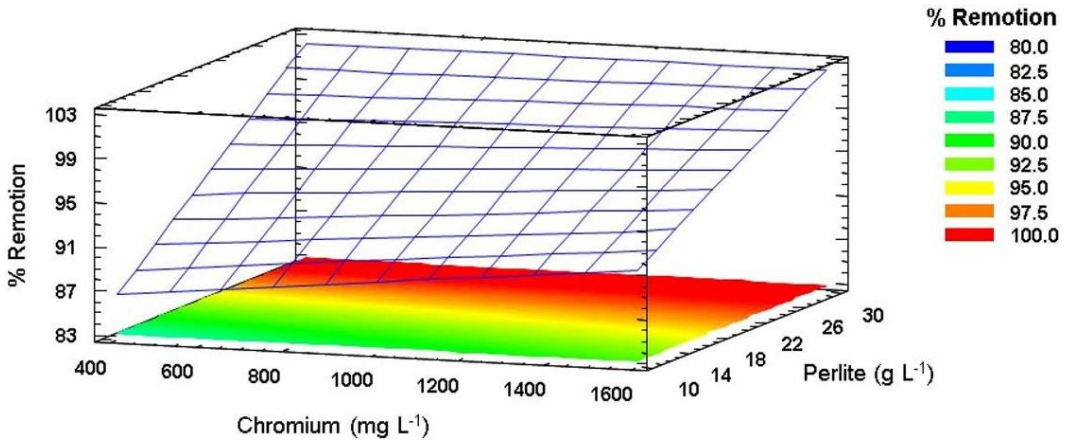

Figure 9. Contours of the Response Surface for chromium removal in percent by adsorption onto activated perlite.

Considering the extreme case from Table 1, for C_0 = 1071 mg L^{-1} (20 g L^{-1}), Ce values ranged from 4.05 to 6.97 mg L^{-1}, confirming that the sum of adsorbed and remaining Cr closely matches the initial amount, thereby validating the consistency of the experimental mass balance.

4. CONCLUSION

The morphological characterization of the expanded perlite revealed grains, scattered particles, expanded laminar structures and compact surfaces of varying sizes. In contrast, the activated perlite exhibited glassy plates with a characteristic honeycomb structure. FTIR analysis confirmed the presence of silicates and hydroxyl functional groups, while XRD patterns indicated an amorphous structure in the expanded perlite and a partial development of crystalline phases upon activation. Additionally, the cation exchange capacity (CEC) increased from 90.57 to 120.52 meq per 100 g, suggesting enhanced ion exchange potential and surface reactivity. Based on both static and dynamic adsorption experiments, the adsorption of chromium onto activated perlite was best described by the Langmuir isotherm model, indicating monolayer adsorption on a homogeneous surface with identical active sites. Kinetic studies showed that equilibrium was reached within approximately eight hours. Both pseudo-first order and pseudo-second-order models provided a good fit to the experimental data, confirming the reliability of the kinetic analysis. Finally, the optimal conditions for maximum chromium removal by activated perlite were established, highlighting its potential as an efficient and low-cost adsorbent for wastewater treatment.

5. DATA AVAILABILITY STATEMENT

The survey data is only available upon request.

6. REFERENCES

ABEWAA, M.; ARKA, A.; HADDIS, T.; MENGISTU, A.; TAKELE, T.; ADINO, E. *et al.* Hexavalent chromium adsorption from aqueous solution utilizing activated carbon developed from Rumex abyssinicus. **Results in Engineering**, v. 22, 2024. https://doi.org/10.1016/J.RINENG.2024.102274

ÁLVAREZ, A. M.; GUERRÓN, D. B.; MONTERO CALDERÓN, C. Natural zeolite as a chromium VI removal agent in tannery effluents. **Heliyon**, v. 7, n. 9, 2021. https://doi.org/10.1016/j.heliyon.2021.e07974

ASANU, M.; BEYENE, D.; BEFEKADU, A. Removal of Hexavalent Chromium from Aqueous Solutions Using Natural Zeolite Coated with Magnetic Nanoparticles: Optimization, Kinetics, and Equilibrium Studies. **Adsorption Science and Technology**, v. 2022, 2022. https://doi.org/10.1155/2022/8625489

AVOLA, T.; CAMPISI, S.; POLITO, L.; ARICI, S.; FERRUTI, L.; GERVASINI, A. Addressing the issue of surface mechanisms and competitive effects in Cr(VI) reductive-adsorption on tin-hydroxyapatite in the presence of co-ions. **Scientific Reports**, v. 13, n. 1, p. 1–14, 2023. https://doi.org/10.1038/S41598-023-44852-7

BAYISA, Y. M.; BULLO, T. A.; AKUMA, D. A. Chromium removal from tannery effluents by adsorption process via activated carbon chat stems (Catha edulis) using response surface methodology. **BMC Research Notes**, v. 14, n. 1, p. 431, 2021. https://doi.org/10.1186/S13104-021-05855-7

BIZUALEM, Y. D.; SHAH, M. A.; IBRAHIMI, S.; GASMI, A.; ELBOUGHDIRI, N. Hydrothermal synthesis and characterization of zsm-5 zeolite from anorthosite: impacts of reaction time and temperature. **Materiali in Tehnologije**, v. 59, n. 1, p. 5–112, 2025. https://doi.org/10.17222/mit.2024.1283

CHANDA, R.; HOSAIN, M.; SUMI, S. A.; SULTANA, M.; ISLAM, S.; BISWAS, B. K. Removal of Chromium (VI) and Lead (II) from Aqueous Solution Using Domestic Rice Husk Ash- (RHA-) Based Zeolite Faujasite. **Adsorption Science & Technology**, v. 2022, 2022. https://doi.org/10.1155/2022/4544611

CORNE, V.; MASKAVIZAN, A. J.; ROMANO, M. S.; CENTURIÓN, E.; GARCÍA, M. DEL C. Adsorción de cromo en materiales arcillosos funcionalizados con compuestos orgánicos. FAO Agris 2019. Available: https://agris.fao.org/search/en/providers/124863/records/671221f10e2cb54d26c2d8ab

DA SILVA FILHO, S. H.; VINACHES, P.; PERGHER, S. B. C. Caracterização estrutural da perlita expandida. **Perspectiva**, v. 41, p. 81–87, 2017.

DE OLIVEIRA, A. G.; JANDORNO, J. C.; DA ROCHA, E. B. D.; DE SOUSA, A. M. F.; DA SILVA, A. L. N. Evaluation of expanded perlite behavior in PS/Perlite composites. **Applied Clay Science**, v. 181, p. 105223, 2019. https://doi.org/10.1016/j.clay.2019.105223

FENG, L.; YI, S.; ZHAO, S.; ZHONG, Q.; REN, F.; LIU, C. *et al.* Recycling of Aluminosilicate-Based Solid Wastes through Alkali-Activation: Preparation, Characterization, and Challenges. **Buildings**, v. 14, n. 1, p. 226, 2024. https://doi.org/10.3390/BUILDINGS14010226

HASHEM, M. A.; NAYEEN, J.; TANVIR HOSSAIN, M.; MUKIMUJJAMAN MIEM, M. Chromium adsorption on thermally activated adsorbent equipped from waste biomass. **Waste Management Bulletin**, v. 2, n. 1, p. 239–249, 2024. https://doi.org/10.1016/J.WMB.2024.01.009

HOU, X.; MA, S.; WANG, X.; OU, Y.; LIU, R. Effects of alkali activation and hydrothermal processes on the transformation of fly ash into Al-substituted tobermorite fiber. **Construction and Building Materials**, v. 397, p. 132372, 2023. https://doi.org/10.1016/j.conbuildmat.2023.132372

HU, G.; YANG, J.; DUAN, X.; FARNOOD, R.; YANG, C.; YANG, J. *et al.* Recent developments and challenges in zeolite-based composite photocatalysts for environmental applications. **Chemical Engineering Journal**, v. 417, p. 129209, 2021. https://doi.org/10.1016/j.cej.2021.129209

HUANCA, P. K.; ANDRADE, C. A.; MAMANI, P. L.; PAREDES, D. J.; PAREDES, B. Obtaining of synthetic zeolite type NaP1 in alkaline medium from natural zeolite under laboratory conditions. **Revista Boliviana de Química**, v. 35, n. 2, p. 46–53, 2018.

HUANG, T.; ZHANG, S.; WEN, L.; FEI, L.; ZHOU, L. Green rust functionalized geopolymer of composite cementitious materials and its application on treating chromate in a holistic system. **Chemosphere**, v. 263, 2021. https://doi.org/10.1016/J.CHEMOSPHERE.2020.128319

ISLAM, I. U.; AHMAD, M.; AHMAD, M.; RUKH, S.; ULLAH, I. Kinetic studies and adsorptive removal of chromium Cr(VI) from contaminated water using green adsorbent prepared from agricultural waste, rice straw. **European Journal of Chemistry**, v. 13, n. 1, p. 78–90, 2022. https://doi.org/10.5155/eurjchem.13.1.78-90.2189

KASAI, M.; KOBAYASHI, Y.; TOGO, M.; NAKAHIRA, A. Synthesis of zeolite-surface-modified perlite and their heavy metal adsorption capability. **Materials Today: Proceedings**, v. 16, p. 232–238, 2019. https://doi.org/10.1016/j.matpr.2019.05.247

KASAI, M.; KOBAYASHI, Y.; YOSHIDA, K.; SASAKI, Y.; TOGO, M.; NAKAHIRA, A. Synthesis and evaluation of zeolite surface-modified perlite. **Journal of the Ceramic Society of Japan**, v. 126, n. 2, p. 115–121, 2018. https://doi.org/10.2109/jcersj2.17155

KERUR, S. S.; BANDEKAR, S.; HANAGADAKAR, M. S.; NANDI, S. S.; RATNAMALA, G. M.; HEGDE, P. G. Removal of hexavalent Chromium-Industry treated water and Wastewater: A review. **Materials Today: Proceedings**, v. 42, p. 1112–1121, 2021. https://doi.org/10.1016/j.matpr.2020.12.492

KHOSHRAFTAR, Z.; MASOUMI, H.; GHAEMI, A. On the performance of perlite as a mineral adsorbent for heavy metals ions and dye removal from industrial wastewater: A review of the state of the art. **Case Studies in Chemical and Environmental Engineering**, v. 8, 100385, 2023. https://doi.org/10.1016/J.CSCEE.2023.100385

KHOSRAVI, R.; MOUSSAVI, G.; GHANEIAN, M. T.; EHRAMPOUSH, M. H.; BARIKBIN, B.; EBRAHIMI, A. A. *et al.* Chromium adsorption from aqueous solution using novel green nanocomposite: Adsorbent characterization, isotherm, kinetic and thermodynamic investigation. **Journal of Molecular Liquids**, v. 256, p. 163–174, 2018. https://doi.org/10.1016/J.MOLLIQ.2018.02.033

KOTWICA, Ł.; PICHÓR, W.; KAPELUSZNA, E.; RÓŻYCKA, A. Utilization of waste expanded perlite as new effective supplementary cementitious material. **Journal of Cleaner Production**, v. 140, p. 1344–1352, 2017. https://doi.org/10.1016/j.jclepro.2016.10.018

KRÓL, M.; MOZGAWA, W.; MORAWSKA, J.; PICHÓR, W. Spectroscopic investigation of hydrothermally synthesized zeolites from expanded perlite. **Microporous and Mesoporous Materials**, v. 196, p. 216–222, 2014. https://doi.org/10.1016/j.micromeso.2014.05.017

KRÓL, MAGDALENA. Natural vs. Synthetic Zeolites. **Crystals**, v. 10, n. 7, p. 622, 2020. https://doi.org/10.3390/CRYST10070622

LAGOS, L. **Bioadsorción de cromo con borra de café en efluentes de una industria curtiembre local**. 2016. 75p. Tesis (Licenciado en Química) – Pontificia Universidad Católica Del Peru, Lima, 2016. Available: https://tesis.pucp.edu.pe/server/api/core/bitstreams/93582d0f-e08e-44ad-83cc-11c2ad9a728b/content

LALA, M. A.; NTAMU, T. E.; ADESINA, O. A.; POPOOLA, L. T.; YUSUFF, A. S.; ADEYI, A. A. Adsorption of hexavalent chromium from aqueous solution using cationic modified rice husk: Parametric optimization via Taguchi design approach. **Scientific African**, v. 20, n. e01633, 2023. https://doi.org/10.1016/J.SCIAF.2023.E01633

LEGORRETA-GARCÍA, F.; VALDEZ-SIERRA, J.; CHÁVEZ-URBIOLA, E. A.; RAMÍREZ-CARDONA, M.; REYES-CRUZ, V. E.; PÉREZ-LABRA, M. Analysis of the transformation of the kaolin from Hidalgo to cancrinite zeolite and secondary phases by the hydrothermal method. **Boletin de la Sociedad Espanola de Ceramica y Vidrio**, 2024. https://doi.org/10.1016/j.bsecv.2024.02.002

LEONARD, J.; SIVALINGAM, S.; SRINADH, R. V.; MISHRA, S. Efficient removal of hexavalent chromium ions from simulated wastewater by functionalized anion exchange resin: Process optimization, isotherm and kinetic studies. **Environmental Chemistry and Ecotoxicology**, v. 5, p. 98–107, 2023. https://doi.org/10.1016/j.enceco.2023.03.001

MCCONNELL, A. A.; EASTWOOD, M. A.; MITCHELL, W. D. Physical characteristics of vegetable foodstuffs that could influence bowel function. **Journal of the Science of Food and Agriculture**, v. 25, n. 12, p. 1457–1464, 1974. https://doi.org/10.1002/jsfa.2740251205

MORADI, L.; MIRZAEI, M.; SASI, H. R. Preparation and characterization of perlite nanoparticles modified with guanidine as an efficient solid base catalyst for the multicomponent synthesis of 1H-pyrazolo [1,2-b] phthalazine-5,10-dione derivatives. **Journal of Molecular Structure**, v. 1263, p. 133124, 2022. https://doi.org/10.1016/j.molstruc.2022.133124

NASIEF, F. M.; SHABAN, M.; ALAMRY, K. A.; KHADRA, M. A.; KHAN, A. A. P.; ASIRI, ABDULLAH, M. *et al.* Hydrothermal synthesis and mechanically activated zeolite material for utilizing the removal of Ca/Mg from aqueous and raw groundwater. **Journal of Environmental Chemical Engineering**, v. 9, n. 5, p. 105834, 2021. https://doi.org/10.1016/j.jece.2021.105834

NEOLAKA, Y. A. B.; LAWA, Y.; NAAT, J.; RIWU, A. A. P.; MANGO, A. W.; DARMOKOESOEMO, H. *et al.* Efficiency of activated natural zeolite-based magnetic composite (ANZ-Fe3O4) as a novel adsorbent for removal of Cr(VI) from wastewater. **Journal of Materials Research and Technology**, v. 18, p. 2896–2909, 2022. https://doi.org/10.1016/j.jmrt.2022.03.153

NJOYA, O.; ZHAO, S.; KONG, X.; SHEN, J.; KANG, J.; WANG, B.; CHEN, Z. Efficiency and potential mechanism of complete Cr(VI) removal in the presence of oxalate by catalytic reduction coupled with membrane filtration. **Separation and Purification Technology**, v. 275, p. 118915, 2021. https://doi.org/10.1016/j.seppur.2021.118915

PAINER, F.; BALDERMANN, A.; GALLIEN, F.; EICHINGER, S.; STEINDL, F.; DOHRMANN, R. *et al.* Synthesis of Zeolites from Fine-Grained Perlite and Their Application as Sorbents. **Materials**, v. 15, n. 13, p. 4474, 2022. https://doi.org/10.3390/MA15134474

PARRA-HUERTAS, R. A.; CALDERÓN-CARVAJAL, C. O.; GÓMEZ-CUASPUD, J. A.; VERA-LÓPEZ, E. Synthesis and characterization of Faujasite-Na from fly ash by the fusion-hydrothermal method. **Boletin de la Sociedad Espanola de Ceramica y Vidrio**, v. 62, n. 6, p. 527–542, 2023. https://doi.org/10.1016/j.bsecv.2023.01.004

PETROVIĆ, R.; LAZAREVIĆ, S.; JANKOVIĆ-ČASTVAN, I.; MATIĆ, T.; MILIVOJEVIĆ, M.; MILOŠEVIĆ, D. V. Removal of trivalent chromium from aqueous solutions by natural clays: Valorization of saturated adsorbents as raw materials in ceramic manufacturing. **Applied Clay Science**, v. 231, p. 106747, 2023. https://doi.org/10.1016/j.clay.2022.106747

PIOQUINTO GARCÍA, S. **Estudio del proceso de adsorción de octametilciclotetrasiloxano en perlita natural y perlita expandida para aplicaciones de purificación de biogás**. 90 p. Universidad Autónoma de Nuevo León, Facultad de Ciencias Químicas, 2018. Available in: http://eprints.uanl.mx/17724/1/1080263183.pdf

RAI, M.; KUMAR, M.; SINGHANIA, R. R.; GIRI, B. S. Tannery waste management and cleaner production of leather in beam house and tanning section: A review. **Bioresource Technology Reports**, v. 30, p. 102116, 2025. https://doi.org/10.1016/j.biteb.2025.102116

SRIVASTAVA, K.; SHRINGI, N.; DEVRA, V.; RANI, A. Pure Silica Extraction from Perlite: Its Characterization and Affecting Factors. **International Journal of Innovative Research in Science, Engineering and Technology**, v. 2, 2013. Available in: https://www.ijirset.com/upload/july/49_%20Pure%20Silica.pdf

TANG, L. J.; XIE, X. Z.; HUANG, Y. X.; PAN, Y.; MI, J. X. Phase diagram for hydrothermal alkali activation of kaolin and quartz: Optimal digestion for the synthesis of zeolites. **Materials Chemistry and Physics**, v. 290, p. 126570, 2022. https://doi.org/10.1016/j.matchemphys.2022.126570

TAYE, A.; MEHRETIE, S.; GETACHEW, N.; ADMASSIE, S. Adsorption of Hexavalent Chromium on KOH Activated Carbon Derived from Water Hyacinth Leaf Coated with Polyaniline/Polypyrrole. **SINET: Ethiopian Journal of Science**, v. 46, n. 3, p. 223–236, 2023. https://doi.org/10.4314/sinet.v46i3.1

TEWELDEBRIHAN, M. D.; DINKA, M. O. Adsorptive Removal of Hexavalent Chromium from Aqueous Solution Utilizing Activated Carbon Developed from Spathodea campanulata. **Sustainable Chemistry**, v. 6, n. 1, p. 8, 2025. https://doi.org/10.3390/suschem6010008

TIAN, Y.; SUN, X.; CHEN, N.; CUI, X.; YU, H.; FENG, Y. *et al.* Efficient removal of hexavalent chromium from wastewater using a novel sodium alginate-biochar composite adsorbent. **Journal of Water Process Engineering**, v. 64, 2024. https://doi.org/10.1016/J.JWPE.2024.105655

VAIOPOULOU, E.; GIKAS, P. Regulations for chromium emissions to the aquatic environment in Europe and elsewhere. **Chemosphere**, v. 254, p. 126876, 2020. https://doi.org/10.1016/j.chemosphere.2020.126876

WANYONYI, F. S.; ORATA, F.; MUTUA, G. K.; ODEY, M. O.; ZAMISA, S.; OGBODO, S. E. *et al.* Application of South African heulandite (HEU) zeolite for the adsorption and removal of Pb2+ and Cd2+ ions from aqueous water solution: Experimental and computational study. **Heliyon**, v. 10, n. 14, 2024. https://doi.org/10.1016/j.heliyon.2024.e34657

ZAHAKIFAR, F.; DASHTINEJAD, M.; SEPEHRIAN, H.; SAMADFAM, M.; FASIHI, J.; YADOLLAHI, A. Intensification of Cr(VI) adsorption using activated carbon adsorbent modified with ammonium persulfate. **Scientific Reports**, v. 14, n. 1, p. 1–12, 2024. https://doi.org/10.1038/S41598-024-68105-3

ZIJUN, Z.; EFFENEY, G.; MILLAR, G. J.; STEPHEN, M. Synthesis and cation exchange capacity of zeolite W from ultra-fine natural zeolite waste. **Environmental Technology & Innovation**, v. 23, p. 101595, 2021. https://doi.org/10.1016/j.eti.2021.101595

ZUO, X.; BALASUBRAMANIAN, R. Evaluation of a novel chitosan polymer-based adsorbent for the removal of chromium (III) in aqueous solutions. **Carbohydrate Polymers**, v. 92, n. 2, 2013. https://doi.org/10.1016/J.CARBPOL.2012.12.009